Strong flux pinning enhancement in $YBa_2Cu_3O_{7-x}$ films by embedded $BaZrO_3$ and $BaTiO_3$ nanoparticles*

Ding Fa-Zhu(丁发柱)†, Gu Hong-Wei(古宏伟)‡, Zhang Teng(张 腾), Wang Hong-Yan(王洪艳), Qu Fei(屈 飞), Qiu Qing-Quan(邱清泉), Dai Shao-Tao(戴少涛), and Peng Xing-Yu(彭星煜)

Key Laboratory of Applied Superconductivity, Chinese Academy of Sciences, Beijing 100190, *China*
Institute of Electrical Engineering, Chinese Academy of Sciences, Beijing 100190, *China*

(Received 5 January 2013; revised manuscript received 22 February 2013)

$YBa_2Cu_3O_{7-x}$ (YBCO) films with embedded $BaZrO_3$ and $BaTiO_3$ nanoparticles were fabricated by metalorganic deposition using trifluoroacetates (TFA-MOD). Both X-ray diffraction and transmission electron microscopy revealed that these $BaZrO_3$ and $BaTiO_3$ nanoparticles had random orientations and were distributed stochastically in the YBCO matrix. The unique combined microstructure enhances the critical current density (J_c) of the $BaZrO_3$/$BaTiO_3$ doped-YBCO films, while keeping the critical transition temperature (T_c) close to that in the pure YBCO films. These results indicate that $BaZrO_3$ and $BaTiO_3$ nanoparticles provide strong flux pinning in YBCO films.

Keywords: $BaZrO_3$ and $BaTiO_3$ nanoparticles, flux pinning, metalorganic deposition using trifluoroacetates

PACS: 74.78.–w, 81.15.Lm **DOI:** 10.1088/1674-1056/22/7/077401

1. Introduction

The electric power applications of high temperature superconductors (HTS) require a high critical current density (J_c) in a magnetic field at 77 K.[1] $YBa_2Cu_3O_{7-x}$ (YBCO)-coated conductors are currently the most researched material for such applications.[2] However, the ability of YBCO-coated conductors to carry currents is significantly reduced in the presence of magnetic fields. In the 1990s, it was found that the most pedestrian factors that limited the critical current density in YBCO were material imperfections and the weak-link effect. Once these problems have been solved, the property that determines the ability of the coated conductors to carry supercurrents is referred to as flux pinning.

It is known that the J_c values of epitaxial YBCO thin films are 10–100 times higher than those of high-quality YBCO bulk single crystals because of the large density of defects inherent from the thin-film growth. The challenge is to discover which of the film defects are most effective at pinning vortices, and how we can introduce relevant defects into the YBCO films. In the early days, nanometer size defects produced by irradiation with electrons, protons, fast neutrons, and ions were introduced as artificial pinning centers.[3–5] However, the introduced irradiation defects were either not effective enough to suppress thermal fluctuations or not commercially feasible. In recent years, many other approaches to obtaining significant improvements in J_c have been realized for YBCO films, including decoration of the substrate surfaces by nanoscaled particles,[6,7] the addition of oxide nanoparticles,[8–12] multilayering of YBCO with second-phase materials,[13–15] mixed rare-earth element doping,[16,17] and intentional deviation from the 123 stoichiometry.[18,19] Among these strategies for enhancing the J_c of YBCO films, the introduction of nanoparticles in YBCO films is the most promising approach because of its valuable advantages such as high efficiency and easy control. MacManus-Driscoll *et al.*[20] first attempted to improve the J_c of YBCO films by introducing $BaZrO_3$ (BZO) nanoparticles in films grown by pulsed laser deposition (PLD). Gutiérrez *et al.*[21] demonstrated that BZO particles in YBCO films grown by metalorganic deposition using trifluoroacetates (TFA-MOD) exhibited a gigantic effectiveness for magnetic flux pinning. In that case, BZO nanodots were randomly dispersed in the YBCO matrix and an overall increase in J_c occurred. In particular, the integration of different nanoparticles leading to a strong vortex-pinning landscape in YBCO superconductors has been reported.[22–24] The critical current density of Y_2O_3/BZO doped-YBCO films has been increased to 6.5 MA/cm^2 at self-field (0 T, 77 K).[22] The results suggest that the combined effects of different structure nanoparticles and defects is desirable for enhancing J_c at low and high fields. In this work, we report greatly enhanced J_c in applied magnetic fields for YBCO films with embedded $BaZrO_3$ and $BaTiO_3$ (BTO) nanoparticles. The correlation between the microstructural features and the superconducting properties is discussed.

*Project supported by the National Natural Science Foundation of China (Grant Nos. 51002149 and 51272250) and the National Basic Research Program of China (Grant No. 2011CBA00105).

†Corresponding author. E-mail: dingfazhu@mail.iee.ac.cn

‡Corresponding author. E-mail: guhw@mail.iee.ac.cn

© 2013 Chinese Physical Society and IOP Publishing Ltd

2. Experimental details

The precursor solution for the YBCO film with BZO and BTO was prepared by dissolving acetates of yttrium, barium, copper, and zirconium, titanium acetylacetonate with stoichiometric proportions in de-ionized water with an excess stoichiometric quantity of trifluoroacetic acid at room temperature. The concentrations of BZO and $BaTiO_3$ in the investigated YBCO films were adjusted by controlling the Zr and the Ti acetylacetonates in the precursor solution, respectively. The resulting aqueous solution was refluxed for 10 h and then dried to a semi-solid state, and then re-dissolved in methanol for drying. Finally, the residue was dissolved in sufficient methanol to get the final trifluoroacetate precursor solution with a concentration of 1.5 mol/L. The solution was coated onto 10 mm×5 mm (00 h)-oriented $LaAlO_3$ (LAO) substrates at a spinning rate of 3000 rpm for 2 min. Then the samples were put in a quartz tube placed in a horizontal furnace. The experimental details of the final heat treatment after drying have been described in Ref. [22].

The film thickness was measured with a Dektak step profiler. The surface morphology of the YBCO film was observed by field emission scanning electron microscopy (FESEM, FEI-Siron). Transmission electron microscopy (TEM) study was carried out using an FEI Tecnai F30 microscope, which was equipped with energy-dispersive spectroscopy (EDS) and operated at 300 kV. The phase and texture of the as-grown film was characterized by X-ray diffraction (XRD) using Cu Kα radiation (Philips X' Pert MRD). Resistive critical transition temperatures (T_c) were measured using the standard four-probe method. A vibrating sample magnetometer (VSM) was used to obtain magnetization J_c data at liquid nitrogen temperature in both self-field and applied magnetic fields. The J_c values of the YBCO films in magnetic fields were determined using the Bean critical state model formula, $J_c(H) = 20\Delta(H)/naba[1-(a/3b)]$, where ΔM is the vertical width of the volume magnetization in units of emu·m^{-3}, n is the thickness of the sample, and a and b are the cross-sectional dimensions of the sample perpendicular to the applied field in units of cm, with $b \geq a$.

3. Results and discussion

The chemical and structural characteristics of the YBCO films prepared using different precursor solutions with the same heat treatment are determined using XRD analysis. Figure 1 shows the XRD θ–2θ diffraction patterns of the samples. It can be seen that all the major diffraction peaks can be indexed as the (00l) reflections of the YBCO phase, which indicates a well-textured, c-axis oriented YBCO grain structure. In addition to the (00l) YBCO peaks, some weak peaks are also observed in curves (ii)–(iv) of Fig. 1. The peaks at the 2θ angles of 31.495° and 45.372° in curve (ii) are assigned to BTO (101) and BTO (200), respectively. The peak at the 2θ angle of 43.238 ° in curve (iii) is assigned to the BZO (200) phase. The BZO (200), BTO (101), and BTO (200) diffraction peaks can be found in the YBCO films prepared using the Ti and Zr acetylacetonate TFA precursor solution, as shown in curve (iv). This demonstrates that the BZO and the BTO phases are indeed formed under the same growth condition as that for the YBCO films.

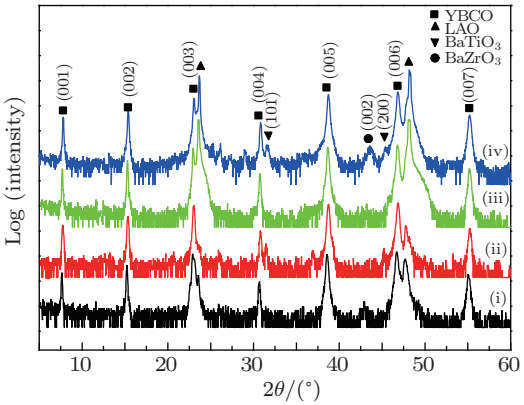


Fig. 1. (color online) XRD θ–2θ diffraction patterns of YBCO films prepared with different solutions: (i) conventional TFA precursor solution, (ii) 11 mol% Ti acetylacetonate TFA precursor solution, (iii) 7 mol% Zr acetylacetonate TFA precursor solution, and (iv) 11 mol% Ti acetylacetonate and 7 mol% Zr acetylacetonate TFA precursor solution.

Figure 2 presents SEM micrographs for the samples shown in Fig. 1. It can be seen that their surface morphologies are significantly different from each other. A smooth surface with few particles is observed in the whole area of the pure YBCO film, as shown in Fig. 2(a). The micrograph of the YBCO film prepared using the Ti-doped TFA precursor solution is shown in Fig. 2(b). We can see that the BTO-doped YBCO film presents many nanoparticles and solid holes (marked by the arrows). These nanoparticles and solid holes are probably the insulating $BaTiO_3$ phase, because the contrast for the particles is probably due to the insulating properties, which cause charging and increased secondary electron emission. The BZO-doped YBCO film presents many nanoparticles with a lateral dimension of 20–50 nm, as shown in Fig. 2(c). It is also found that some BZO nanoparticles connect together. Figure 2(d) shows the SEM micrograph of the YBCO film prepared using the 11.0 mol% Ti acetylacetonate and 7.0 mol% Zr acetylacetonate TFA precursor solution. It can be clearly seen that the density of particles on the YBCO film surface is larger than that on the other samples. And these particles are found to be distributed uniformly across the film surface rather than clustered together.

Figure 3 is the cross-sectional TEM image and EDS mapping of the YBCO film co-doped with 7 mol% BZO and 11 mol% BTO, which clearly show the nanoparticles on the

YBCO surface and the nanorods at the substrate interface. The compositions of these particles are confirmed by EDS spectra. It is observed from Fig. 3(a) that the nanoparticles in the film have high concentrations of Ba, Zr, and O, and are Cu deficient. The Zr is not detectable in other areas. From the EDS spectra in Fig. 3(b), we find that the nanorods at the substrate interface have a high concentration of Ti. These results suggest that these nanoparticles and nanorods are BZO and BTO, respectively. Figure 3(b) is a high-resolution TEM (HRTEM) image of a BTO nanorod, showing nucleation and growth starting from the substrate surface. This image shows the distortion due to short stacking faults in the YBCO matrix near the interface with the nanorods. Small regions of amorphous material also present at various points along the sides of the nanorods. From this image it is also clearly seen that the particle and the matrix are not coherent.

A cross-sectional HRTEM image of the BZO/BTO doped YBCO film is shown in Fig. 4(a). The corresponding selected-area electron diffraction (SAED) patterns in Figs. 4(b) and 4(c) confirm the *c*-axis orientation and the good alignment of the BZO/BTO-doped YBCO film towards the substrate.

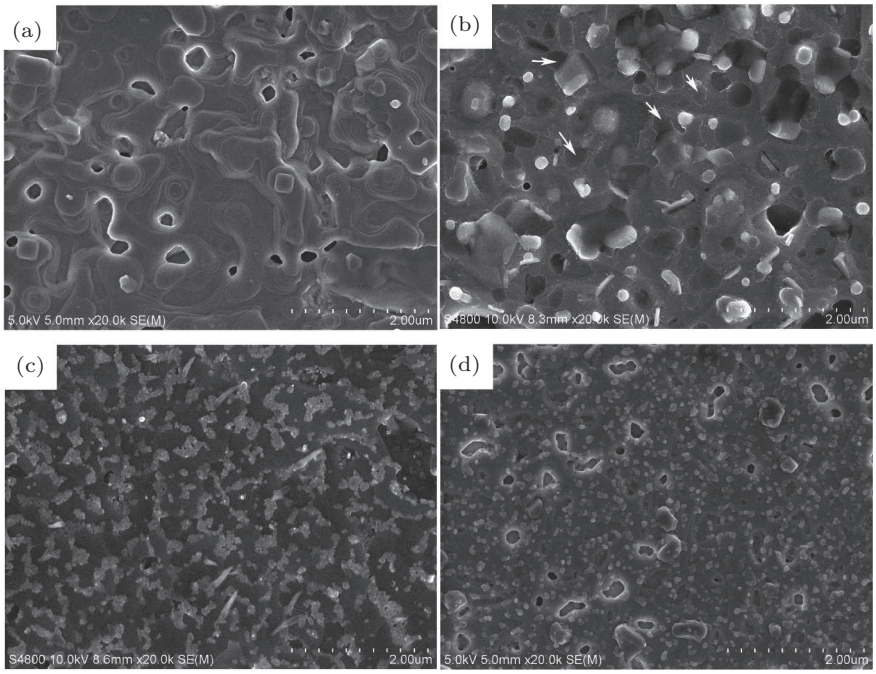


Fig. 2. SEM micrographs of YBCO films prepared with different solutions: (a) conventional TFA precursor solution, (b) 11 mol% Ti acetylacetonate TFA precursor solution, (c) 7 mol% Zr acetylacetonate TFA precursor solution, and (d) 11 mol% Ti acetylacetonate and 7 mol% Zr acetylacetonate TFA precursor solution.

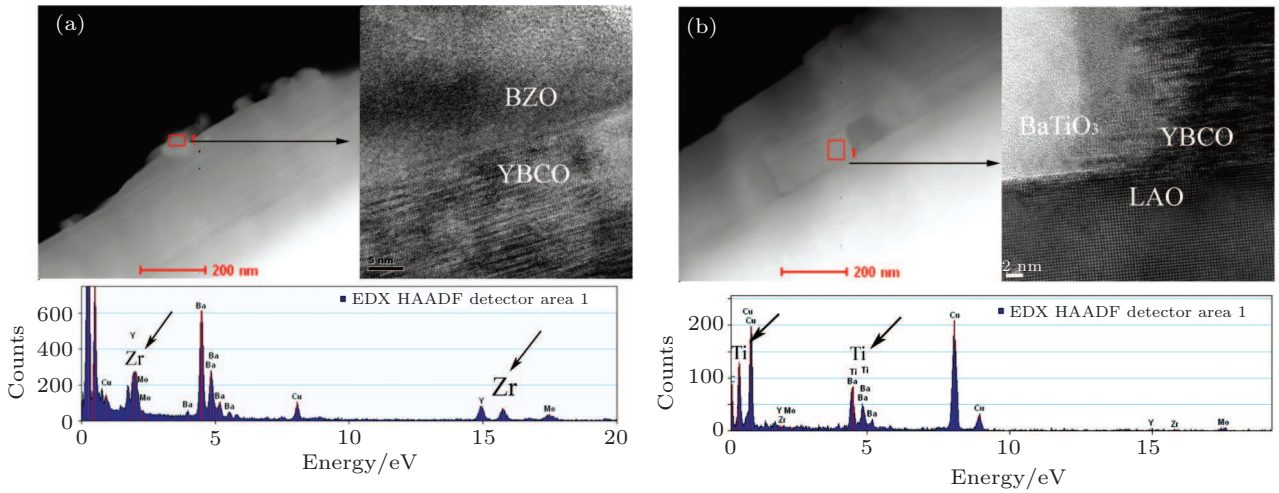


Fig. 3. (color online) TEM image and EDS mappings of the BZO/BTO-doped YBCO film: (a) BZO nanoparticles in the film, (b) BTO nanocolumns in the film.

The T_c values of the YBCO samples are measured using the four-probe method, as shown in Fig. 5. The T_c of the BZO/BTO-doped YBCO film is about 90 K, indicating that there are few effects of the BZO and BTO particles on the YBCO matrix in these solution-derived YBCO composite films. Moreover, the transition width (ΔT) of these YBCO films is smaller than 1 K, which suggests the high homogeneity within the films.

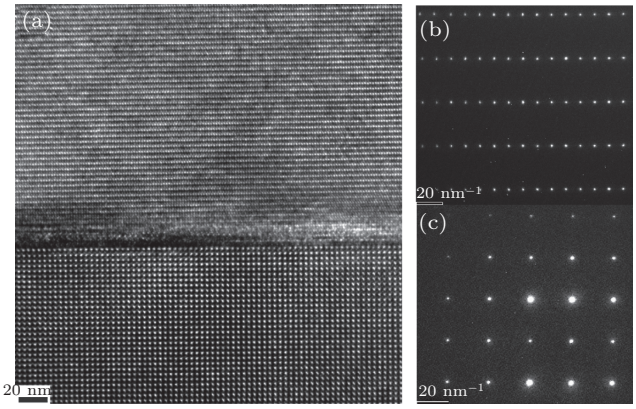


Fig. 4. (a) HRTEM image of the BZO/BTO-doped YBCO film, (b) SAED pattern of the YBCO film, and (c) SAED pattern of the $LaAlO_3$ substrate.

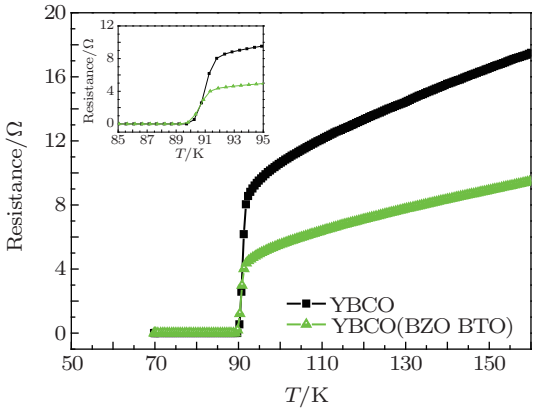


Fig. 5. (color online) The dependence of normalized resistivity R on temperature T for the pure YBCO film and the BZO/BTO-doped YBCO film; the inset shows the results near T_c.

Figure 6 shows the field dependence of the magnetization J_c of the YBCO films at 77 K with the fields parallel to the c axis. For comparison, data from a standard MOD-YBCO film and a BTO-doped YBCO film on an LAO substrate are also plotted in the figure. The self-field J_c values for the BTO-doped YBCO film and the BZO/BTO-doped YBCO film are 5.0 MA/cm^2 and 6.5 MA/cm^2, respectively. The J_c of the BZO/BTO-doped YBCO film is improved significantly in high fields. For instance, the J_c of the BZO/BTO-doped YBCO film is increased tenfold in 1 T compared to that of the BTO-doped YBCO film. A significant increase in the irreversibility field H_{irr} to 8 T is also observed. These results strongly suggest that the enhanced pinning for all magnetic fields results from the BZO and BTO nanoparticles doping in the YBCO matrix. Combining with Figs. 2 and 3, it is evident that the critical current density of the YBCO film is very sensitive to the size, density, and distribution of the additions. The size of the particles in the BZO/BTO-doped YBCO film is between 10 nm and 40 nm, and these particles are distributed uniformly across the film surface. So, the strongly enhanced flux pinning over a wide range of magnetic fields can be attributed to the introduction of both BZO and BTO nanoparticles.

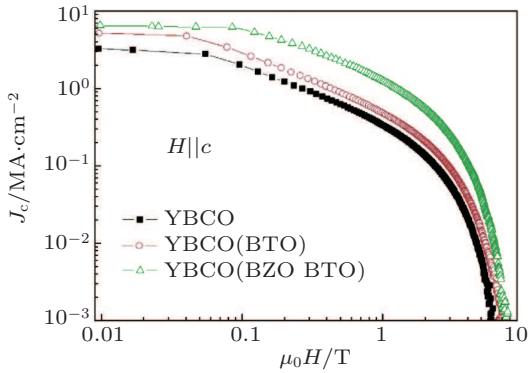


Fig. 6. (color online) Critical current density versus magnetic field parallel to the c axis at 77 K for the pure YBCO film, the BTO-doped YBCO film, and the BZO/BTO-doped YBCO film.

4. Conclusion

In summary, we have demonstrated the ability to significantly enhance the performance of YBCO films in applied magnetic fields with the introduction of BTO and BZO nanorods. The BZO/BTO-doped YBCO films have high densities of nanoparticles, nanocolumns, and stacking faults. The critical current density in magnetic fields up to 8 T reveals a strong enhancement of J_c at high magnetic fields with these different nanostructures of precipitates and related stacking faults. The BZO/BTO-doped YBCO films have a T_c of over 90 K and ΔT lower than 1 K, indicating few effects of the introduced BZO and BTO particles on the YBCO matrix.

Acknowledgment

The authors thank Professor Zhang Xi-Xiang for help in the TEM study at the King Abdullah University of Science and Technology, Saudi Arabia.

References

[1] Larbalestier D C, Gurevich A, Feldmann D M and Polyanskii A 2001 *Nature* **414** 368
[2] Iijima Y, Tanabe N, Kohno O and Ikeno Y 1992 *Appl. Phys. Lett.* **60** 769
[3] Dover R B, Gyorgy E M, Schneemeyer L F, Michell J W, Rao K V, Puzniak R and Waszczia J V 1989 *Nature* **342** 55
[4] Civale L, Marwick A D, McElfresh M W, Worthington T K, Malozemoff A P and Holtzberg F H 1990 *Phys. Rev. Lett.* **65** 1164
[5] Sauerzopf F M, Wiesinger H P, Kritscha W, Weber H W, Crabtree G W and Liu J Z 1991 *Phys. Rev. B* **43** 3091
[6] Gutierrez J, Puig T, Gibert M, Moreno C, Roma N, Pomar A and Obradors X 2009 *Appl. Phys. Lett.* **94** 172513

[7] Polat Ö, Ertugrul M, Thompson J R, Leonard K J, Sinclair J W, Paranthaman M P, Wee S H, Zuev Y L, Xiong X, Selvamanickam V, Christen D K and Aytug T 2012 *Supercond. Sci. Technol.* **25** 025018
[8] Maiorov B, Baily S A, Zhou H, Ugurlu O, Kennison J A, Dowden P C, Holesinger T G, Foltyn S R and Civale L 2009 *Nature Mater.* **8** 398
[9] Engel S, Thersleff T, Hühne R, Schultz L and Holzapfel B 2007 *Appl. Phys. Lett.* **90** 102505
[10] Varanasi C V, Barnes P N, Burke J, Brunke L, Maartense I, Haugan T J, Stinzianni E A, Dunn K A and Haldar P 2006 *Supercond. Sci. Technol.* **19** L37
[11] Varanasi C V, Burke J, Brunke L, Wang H, Sumption M and Barnes P N 2007 *J. Appl. Phys.* **102** 063909
[12] Hanisch J, Cai C, Huhne R, Schultz L and Holzapfel B 2005 *Appl. Phys. Lett.* **86** 122508
[13] Haugan T, Barnes P N, Wheeler R, Meisenkothen F and Sumption M 2004 *Nature* **430** 867
[14] Kiessling A, Hänisch J, Thersleff T, Reich E, Weigand M, Hühne R, Sparing M, Holzapfel B, Durrell J H and Schultz1 L 2011 *Supercond. Sci. Technol.* **24** 055018
[15] Peng L, Cai C, Chen C, Liu Z, Liu J, Gao B and Zhang J 2008 *J. Phys. D: Appl. Phys.* **41** 155403
[16] Barnes P N, Kell J W, Harrison B C, Haugan T J, Varanasi C V, Rane M and Ramos F 2006 *Appl. Phys. Lett.* **89** 012503
[17] Li P L, Wang Y Y, Tian Y T, Wang J, Niu X L, Wang J X, Wang D D and Wang X X 2008 *Chin. Phys. B* **17** 3484
[18] Lee S Y, Song S and Kim B J 2006 *Physica C* **445–448** 578
[19] Ding F Z, Gu H W, Zhang T, Dai S T and Xiao L Y 2011 *Chin. Phys. B* **20** 027402
[20] MacManus-Driscoll J L, Foltyn S R, Jia Q X, Wang H, Serquis A, Civale L, Maiorov B, Hawley M E, Maley M P and Peterson D E 2004 *Nature Mater.* **3** 439
[21] Gutiérrez J, Llordés A, Gázquez J, Gibert M, Romà N, Ricart S, Pomar A, Sanditmenge F, Mestres N, Puig T and Obradors X 2007 *Nature Mater.* **6** 367
[22] Ding F, Gu H, Zhang T, Wang H, Qu F, Dai S, Peng X and Cao J 2012 *J. Alloys Compd.* **513** 277
[23] Feldmann D M, Holesinger T G, Maiorov B, Zhou H, Foltyn S R, Coulter J Y and Apodoca I 2010 *Supercond. Sci. Technol.* **23** 115016
[24] Mikheenko P, Dang V S, Tse Y Y, AwangKechik M M, Paturi P, Huhtinen H, Wang Y, Sarkar A, Abell J S and Crisan A 2010 *Supercond. Sci. Technol.* **23** 125007